AIAA JOURNAL
Vol. 33, No. 4, April 1995

Time-Marching Analysis of Fluid-Coupled Systems with Large Added Mass

F. Belanger* and M. P. Païdoussis†
McGill University, Montreal, Quebec H3A 2K6, Canada
and
E. de Langre‡
CEA-CEN Saclay, DMT/SEMT/VIBR, Gif-sur-Yvette 91191, France

Time-marching stability analysis of fluid–structure interaction problems is considered in this paper. The Navier–Stokes equations and the equation of motion of the structure are integrated simultaneously in time in a coupled manner to assess structural dynamics and thereby the possibility for flutter and/or divergence. A method developed by the authors for the incompressible Navier–Stokes equations consists of combining a Runge–Kutta time integration for the structure with a three-point backward time discretization for the fluid. Problems have been encountered with that method, however, when the fluid-added mass is larger than the structural mass, leading to numerical instability in the integration scheme. A cure to remedy these difficulties is proposed in this paper. It consists of introducing estimates for the added mass, obtained, for example, from potential flow calculations, into the structural equation so as to cancel the fluid inertial forces. To illustrate the possibilities of the method, analysis of the free vibrations of two coaxial cylinders coupled by annular fluid is performed.

Introduction

METHODS to study fluid–structure interaction problems by simultaneous time integration of the fluid and structural equations have been developed more systematically in recent years by making use of computational fluid dynamics techniques. Nomura and Hughes[1] applied the finite element method, for example, to study the free vibrations of a cylinder in confined and unconfined incompressible flow, whereas examples of the application of the finite volume method to time-marching aeroelastic analyses may be found in Ref. 2, where Rausch et al. simulated flutter results using an appropriately adapted Euler code. Farhat[3] investigated aeroelastic instability phenomena on moving grids.

A method for structural dynamics and stability analysis in incompressible laminar flow has also been developed by the authors.[4] The analysis is performed in the time domain. A small initial displacement is given to a fluid-coupled structure before releasing it; its free vibrations are then tracked in time by integrating simultaneously the Navier–Stokes and structural equations.

Referring to Fig. 1, the method has been applied to the stability analysis of two coaxial cylinders in annular flow. A portion of the outer cylinder undergoes one-degree-of-freedom rigid-body lateral vibrations in one plane, a motion coupled to the fluid flowing in the annular passage, the inner boundary of which is delimited by a fixed cylinder of generally varying cross section. The cylinder was shown to be subject to divergence instability. The mass of the vibrating cylinder was approximately two times larger than the fluid-added mass of the annular fluid.

It is shown in this paper that the coupled time integration method is numerically unstable when the added mass is larger than the structural mass. This can typically be the case in highly confined annular geometries with a high-density fluid, unlike in other aeroelastic applications where the external fluid is air and the corresponding added masses are small. A special procedure must be devised to deal with these numerical problems, and one such procedure is proposed here.

Received June 8, 1994; presented as Paper 94-2267 at the 25th AIAA Fluid Dynamics Conference, Colorado Springs, CO, June 20–23, 1994; revision received Nov. 30, 1994; accepted for publication Nov. 30, 1994.

*Research Associate, Department of Mechanical Engineering, currently at CAE Electronics Ltd, C.P. 1800, Ville St-Laurent, Quebec H4L 4X4, Canada. Member AIAA.
†Thomas Workman Professor, Department of Mechanical Engineering.
‡Chief, Laboratoire des Vibrations.

Coupled Fluid and Structural Integration

The Navier–Stokes and continuity equations for a laminar flow of incompressible fluid are written in nondimensional form as

$$\frac{\partial \boldsymbol{U}}{\partial t} + \boldsymbol{G}(\boldsymbol{U}, p) = 0, \qquad \nabla \cdot \boldsymbol{U} = 0 \tag{1}$$

where

$$\boldsymbol{G}(\boldsymbol{U}, p) = \nabla \cdot \boldsymbol{U}\boldsymbol{U} + \nabla p - \frac{1}{Re}\nabla^2 \boldsymbol{U} \tag{2}$$

The Reynolds number Re is defined for each specific problem in terms of a characteristic length and velocity; $\boldsymbol{U}$ is the velocity vector of the fluid and p is the pressure.

Assuming the solution for the fluid is known at the time levels t^k, $k \leq n$, where the time increment is given by $\Delta t = t^n - t^{n-1}$, the following two second-order discretizations for the time derivative,

$$\left(\frac{\partial \boldsymbol{U}}{\partial t}\right)^{n+\frac{1}{2}} = \frac{8\boldsymbol{U}^{n+\frac{1}{2}} - 9\boldsymbol{U}^n + \boldsymbol{U}^{n-1}}{3\,\Delta t}$$
$$\left(\frac{\partial \boldsymbol{U}}{\partial t}\right)^{n+1} = \frac{3\boldsymbol{U}^{n+1} - 4\boldsymbol{U}^n + \boldsymbol{U}^{n-1}}{2\,\Delta t} \tag{3}$$

may be used to advance the solution from t^n to $t^{n+\frac{1}{2}}$ or from t^n to t^{n+1}, respectively; both will actually be required in the integration scheme adopted for the structure, to be introduced shortly. The semidiscretized momentum equation and the continuity equation become, after introducing Eq. (3) in Eq. (1) and rearranging,

$$\boldsymbol{U}^{n+1/2} + (3\,\Delta t/8)\boldsymbol{G}^{n+\frac{1}{2}} = (9\boldsymbol{U}^n - \boldsymbol{U}^{n-1})/8$$
$$\nabla \cdot \boldsymbol{U}^{n+\frac{1}{2}} = 0 \tag{4}$$

$$\boldsymbol{U}^{n+1} + (2\,\Delta t/3)\boldsymbol{G}^{n+1} = (4\boldsymbol{U}^n - \boldsymbol{U}^{n-1})/3$$
$$\nabla \cdot \boldsymbol{U}^{n+1} = 0 \tag{5}$$

where $\boldsymbol{G}^{n+\frac{1}{2}} = \boldsymbol{G}(\boldsymbol{U}^{n+\frac{1}{2}}, p^{n+\frac{1}{2}})$, $\boldsymbol{G}^{n+1} = \boldsymbol{G}(\boldsymbol{U}^{n+1}, p^{n+1})$. Solutions to the implicit systems of nonhomogeneous Eqs. (4) or (5), respectively, for $(\boldsymbol{U}^{n+\frac{1}{2}}, p^{n+\frac{1}{2}})$ or $(\boldsymbol{U}^{n+1}, p^{n+1})$, may then proceed using, for example, the method of artificial compressibility, described in Refs. 5–7 in conjunction with various space discretization schemes.

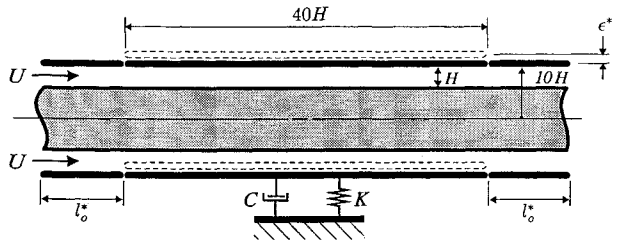

Fig. 1 Annular geometry with vibrating central portion of outer cylinder.

The actual procedure adopted in the present paper is that of Refs. 5 and 7, where details may be found, in particular as regards the finite differences used for the space discretization.

No-slip boundary conditions are imposed in solving Eq. (4) [or Eq. (5)]. This implies that the velocity of the wall must be known at $t^{n+\frac{1}{2}}$. However, it is noted that in a numerical fluid–structure procedure the displacement of the wall must also be known in advance to solve Eq. (4), as it serves in redefining the fluid domain in which the solution is defined at $t^{n+\frac{1}{2}}$. Hence, for the present purposes we consider that the fluid solution at $t^{n+\frac{1}{2}}$ and, in particular, the fluid force $F^{n+\frac{1}{2}}$ acting on the structure are functions of the displacement and velocity of the walls at $t^{n+\frac{1}{2}}$, i.e., $F^{n+\frac{1}{2}} \equiv F(\epsilon^{n+\frac{1}{2}}, \dot{\epsilon}^{n+\frac{1}{2}})$, where ϵ and $\dot{\epsilon}$ are some modal wall displacement and velocity, respectively. The considerations of this paragraph also apply in going from t^n to t^{n+1} when solving Eq. (5).

In the present paper, the procedure described in Ref. 4 to solve the flow problem is employed. Small structural vibrations are considered to allow for performing the flow computations on fixed meshes with a resulting small error in the spatial discretization. Wall motion is taken into account by Taylor series expansion of the boundary conditions, which are linearized to obtain the fluid velocity imposed at the fixed mesh boundary; these are transpiration-type boundary conditions, a general derivation of which may be found in Ref. 4, where the details required for implementing them in the present problem are also given.

Now, the annular geometry is shown in Fig. 1. The mechanical system consists of a portion of the outer cylinder that is free to vibrate transversely as a rigid body in one plane, its displacement being denoted by $\epsilon^*(t^*)$. This cylinder is restrained by a spring K and a dashpot C; it is of length $40H$, radius $10H$, and mass M and is delimited upstream and downstream by two fixed cylinders of radius $10H$ and length $l_0^* = 40H$. The inner cylinder, of radius $9H$, is stationary. In the absence of vibrations of the outer cylinder, there is steady, axisymmetric flow in the annular region; U denotes the mean flow velocity at the upstream inlet.

Here, H and U will be the characteristic length and velocity used to nondimensionalize the equations. Throughout the paper, starred quantities will be dimensional and nonstarred ones nondimensional, with the following important exceptions: H and U, as well as the structural quantities M, C, and K, and ν and ρ (defined below) are understood to be dimensional. Hence, in Eqs. (1) and (2) we have

$$U = \frac{U^*}{U}, \qquad p = \frac{p^*}{\rho U^2}, \qquad t = \frac{H t^*}{U}$$
$$\nabla = H\nabla^*, \qquad Re = \frac{UH}{\nu} \tag{6}$$

where ρ and ν are the fluid density and fluid kinematic viscosity and ∇ is the nabla operator.

The equation of motion of the vibrating cylinder may be written in nondimensional form as

$$\ddot{\epsilon}(t) = -2\zeta\omega_n\dot{\epsilon}(t) - \omega_n^2\epsilon(t) + \sigma F(\epsilon, \dot{\epsilon}) \tag{7}$$

where

$$\epsilon = \frac{\epsilon^*}{H}, \qquad \omega_n = \sqrt{\frac{K}{M}}\frac{H}{U} \equiv \omega_n^*\frac{H}{U}, \qquad \zeta = \frac{C}{2\sqrt{KM}}$$
$$\sigma = \frac{\rho H^3}{M}, \qquad F = \frac{F^*}{\rho U^2 H^2} \tag{8}$$

and in which $\omega_n^* = \sqrt{K/M}$. A dot denotes a time derivative, ω_n and ζ are the dimensionless natural frequency and the reduced damping of the system, and σ is a factor weighting the relative contribution of the fluid and mechanical forces. In keeping with the discussion above, the fluid-coupling force exerted on the cylinder, $F(\epsilon, \dot{\epsilon})$, has been expressed as a function of ϵ and $\dot{\epsilon}$, which is symbolic of the way in which it is obtained numerically.

Notice that in studying the dynamics of the cylinder, $C = 0$ will be taken ($\zeta = 0$); thus, any damping in the free vibrations will originate from fluid effects.

Assuming that the displacement ϵ^n, velocity $\dot{\epsilon}^n$, and acceleration $\ddot{\epsilon}^n$ of the structure at time t^n are known, the integration of Eq. (7) may be defined using a second-order Runge–Kutta scheme, by the following sequence:

Predictor step

$$\epsilon^{n+\frac{1}{2}} = \epsilon^n + (\Delta t/2)\dot{\epsilon}^n$$
$$\dot{\epsilon}^{n+\frac{1}{2}} = \dot{\epsilon}^n + (\Delta t/2)\,\ddot{\epsilon}^n$$
$$F^{n+\frac{1}{2}} = F\left(\epsilon^{n+\frac{1}{2}}, \dot{\epsilon}^{n+\frac{1}{2}}\right) \tag{9}$$
$$\ddot{\epsilon}^{n+\frac{1}{2}} = -2\zeta\omega_n\dot{\epsilon}^{n+\frac{1}{2}} - \omega_n^2\epsilon^{n+\frac{1}{2}} + \sigma F^{n+\frac{1}{2}}$$

Corrector step

$$\epsilon^{n+1} = \epsilon^n + \Delta t\,\dot{\epsilon}^{n+\frac{1}{2}}$$
$$\dot{\epsilon}^{n+1} = \dot{\epsilon}^n + \Delta t\,\ddot{\epsilon}^{n+\frac{1}{2}}$$
$$F^{n+1} = F(\epsilon^{n+1}, \dot{\epsilon}^{n+1}) \tag{10}$$
$$\ddot{\epsilon}^{n+1} = -2\zeta\omega_n\dot{\epsilon}^{n+1} - \omega_n^2\,\epsilon^{n+1} + \sigma F^{n+1}$$

As seen in the predictor step, the intermediate values $\epsilon^{n+\frac{1}{2}}$ and $\dot{\epsilon}^{n+\frac{1}{2}}$ for displacement and velocity of the structure are first determined at $t^{n+\frac{1}{2}} = t^n + \Delta t/2$, independently of the flow problem; they serve in deriving the boundary conditions necessary to integrate and advance the Navier–Stokes equations to $t^{n+\frac{1}{2}}$ by using the time-discretized form (4), which allows for the calculation of the fluid force $F^{n+\frac{1}{2}}$ (see Ref. 4). The acceleration, $\ddot{\epsilon}^{n+\frac{1}{2}}$ is then obtained from the structural equation [last equation in Eqs. (9)], and the solution can proceed to the corrector step, which is solved in a similar manner for the variables ϵ^{n+1}, $\dot{\epsilon}^{n+1}$, and $\ddot{\epsilon}^{n+1}$, by using the time-discretized form (5) for the flow equations.

It is to be noticed that this fluid–structure time integration method treats the fluid equations implicitly [Eqs. (4) and (5)] and the structural equations explicitly [Eqs. (9) and (10)]. This has advantages in regard to the time steps allowed for the coupled system. Indeed, even though quite different characteristics between fluid and structural system coefficient matrices are involved (which would require, for all practical applications, that a much smaller time step be chosen for the fluid as compared to the structural integration if the former were also performed explictly), treating the fluid implicitly allows to match more appropriately the coupled integration time steps of fluid and structure.

Application to Two-Dimensional Annular Geometry

As a first application, we consider that the vibrating outer cylinder in Fig. 1 is infinitely long, in which case the problem is two dimensional. The fluid dynamics is independent of whether or not there is any axial flow and only takes place in the (r, θ) plane. The characteristic velocity can no longer be chosen as U, and we select $\omega_n^* H$ instead for that purpose, where ω_n^* is, as before, the (dimensional) natural frequency of the in vacuo mass–spring system; hence the Reynolds number in Eqs. (2) and (6) is replaced by the Stokes number S, where

$$S = \frac{\omega_n^* H^2}{\nu} \tag{11}$$

Similarly to the Reynolds number, S is a measure of the relative importance of the inertial and viscous forces.

The structural quantities M, C, and K, as well as the fluid force F, are all defined per unit length and are denotedby lowercase letters, namely m, c, k, and f. Hence we now have the following definitions in Eq. (7):

$$\epsilon = \frac{\epsilon^*}{H}, \qquad \omega_n = \sqrt{\frac{k}{m}}\frac{H}{\omega_n^* H} = 1, \qquad \zeta = \frac{c}{2\sqrt{km}}$$
$$\sigma = \frac{\rho H^2}{m}, \qquad f = \frac{f^*}{\rho \omega_n^{*2} H^3} \tag{12}$$

and we remark that $\omega_n = 1$.

The nondimensional potential fluid-added mass per unit length for this problem, denoted by m_{ap}, may be obtained analytically[8,9] (subscripts p and v will denote potential and viscous values, respectively); it is given in terms of the dimensional added mass m_{ap}^* by

$$m_{ap} = \frac{m_{ap}^*}{\rho H^2} = \pi r_o^2 \frac{(r_o/r_i)^2 + 1}{(r_o/r_i)^2 - 1} \tag{13}$$

where r_o and r_i are the nondimensional radii of the outer and inner cylinders, respectively 10 and 9 in this numerical example. Remark that the actual viscous added mass m_{av} is larger than the potential value by roughly 20% at low vibration frequency, and it tends to the potential value as the vibration frequency increases.[4] Combining Eqs. (12) and (13) for σ, we have

$$\sigma = \frac{1}{m_{ap}}\frac{1}{m/m_{ap}^*} \tag{14}$$

Calculations were performed at two Stokes numbers, namely at $S = 3$ in Fig. 2 and at $S = 300$ in Fig. 3, for various values of σ. Since the nondimensional potential added mass m_{ap} in Eq. (14) is a constant geometric parameter that, for this geometry, is equal to 2993 by Eq. (13), the value of σ was varied by changing the ratio of structural mass to dimensional potential fluid-added mass m/m_{ap}^*, as per Eq. (14). The results in Figs. 2 and 3 are for $m/m_{ap}^* = 100, 10, 3, 1$. Only the solid lines are to be considered for the moment, these being referred to as non–fluid inertia compensated (NFIC), a notation defined in the next section.

Thus, after giving a small initial displacement to the outer cylinder, equal to $0.1H$, and releasing it, its equation of motion (7) was integrated simultaneously with the Navier–Stokes equations. The time step Δt was chosen according to the formula

$$\Delta t = \frac{2\pi}{40\omega_n} = \frac{2\pi}{40} \tag{15}$$

where the last identity is obtained by remembering that $\omega_n = 1$ [see Eq. (12)]. The vibration period of the fluid-coupled cylinder will be larger than that of the in vacuo mass–spring system as a result of the added mass, and this will ensure that we have at least 40 time steps per vibration cycle. The mesh used in those calculations had 24 points stretched in the radial direction; no mesh points were required in the circumferential direction θ, which was eliminated by using a spectral Galerkin method with Fourier expansions.[4]

In Figs. 2 and 3 it is seen that, for a given ratio m/m_{ap}^*, the free vibrations become more damped as the Stokes number is lowered, because the viscous effects are then more predominant. Also, for a given Stokes number, the vibrations are more damped and the vibration period is larger when the ratio m/m_{ap}^* diminishes, indicating the increased weighting of the fluid forces as compared to the mechanical ones. When the potential and structural masses are equal, $m/m_{ap}^* = 1$, at which point, as mentioned previously, the actual viscous added mass m_{av}^* is larger than m, divergence instability of the cylinder is observed in both Figs. 2 and 3 (solid line, left-hand end of figures). This, however, cannot be physically meaningful, as no fluid-elastic effects are likely to cause an instability in a problem in which only damped vibrations are significant. Hence this is essentially a numerical instability encountered when the fluid inertial forces become larger than the mechanical ones. The purpose of the next section will be to devise a means to fix this numerical problem.

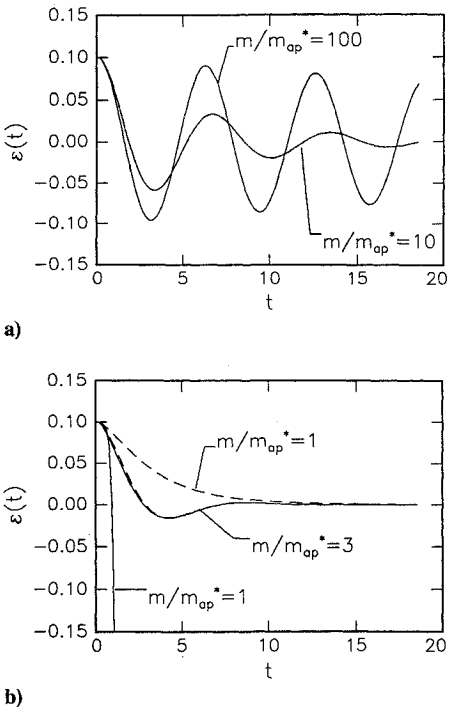

Fig. 2 Free-vibration time history obtained at Stokes number of S = 3 (two-dimensional geometry) for various ratios of cylinder mass to potential fluid-added mass, m/m_{ap}^*: ——, non–fluid inertia compensated (NFIC) results; - - -, fluid inertia compensated (FIC) results.

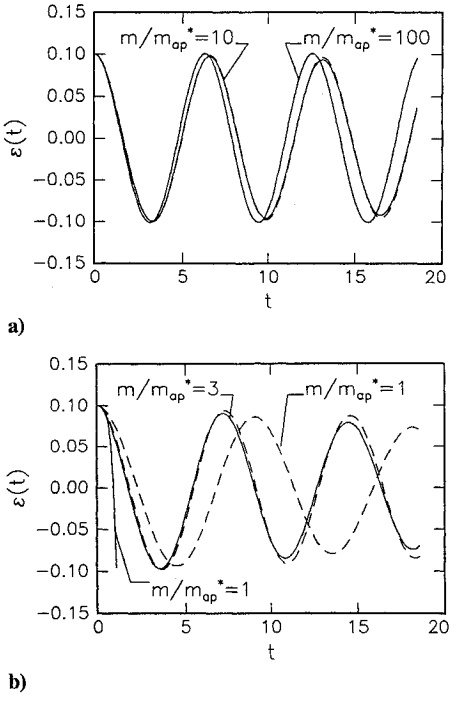

Fig. 3 Free-vibration time history obtained at Stokes number of S = 300 (two-dimensional geometry) for various ratios of cylinder mass to potential fluid-added mass, m/m_{ap}^*: ——, NFIC results; - - -, FIC results.

Before this is accomplished, however, an investigation will be carried out to assess whether the time step chosen in the present problem is appropriate. For that purpose, computations were performed at $S = 300$, $m/m_{ap}^* = 100$, whereas the time step was varied by selecting $\Delta t = 2\pi/20$, $2\pi/30$, $2\pi/40$ [see Eq. (15)]. The results, shown in Fig. 4, are seen to be all nearly perfectly superimposed, especially as regards the time steps $\Delta t = 2\pi/30$ and $\Delta t = 2\pi/40$. Similar results were also obtained in computations performed for the three-dimensional problem discussed later

in this paper. These favorable conclusions follow because of the implicit treatment adopted for the Navier–Stokes equations. It may also be mentioned that the accuracy of the method in regard to the spatial discretization has been analyzed in Ref. 4 through comparison with analytical results for the two-dimensional problem and by performing mesh refinement studies for the three-dimensional problem. The numerical method performed satisfactorily also in this respect.

Fluid Inertia Compensated Procedure

The procedure used to correct for the detrimental effect that a large added mass has on the numerical time integration method employed for the structure is the following. We remark first that the fluid force inertial component in Eq. (7) may be written, by definition, to be proportional to $-M^*_{av}\ddot{\epsilon}^*$ or, in nondimensional form, $-\sigma M_{av}\ddot{\epsilon}$, where the dimensionless viscous fluid-added mass in the three-dimensional problem is given by $M_{av} = M^*_{av}/\rho H^3$. Then, using an estimate for M_{av}, which we denote by $\hat{M}_a$, we subtract the corresponding estimated fluid inertial force $-\sigma\hat{M}_a\ddot{\epsilon}$ from both sides of Eq. (7) to obtain

$$(1+\sigma\hat{M}_a)\ddot{\epsilon}(t) = -2\zeta\omega_n\dot{\epsilon}(t) - \omega_n^2\epsilon(t) + \sigma\hat{F}(\epsilon,\ \dot{\epsilon},\ \ddot{\epsilon}) \tag{16}$$

where

$$\hat{F}(\epsilon,\dot{\epsilon},\ddot{\epsilon}) = F(\epsilon,\dot{\epsilon}) + \hat{M}_a\ddot{\epsilon} \tag{17}$$

The resulting equivalent mass on the structure side of the equation (left-hand side) now becomes larger than the fluid-added mass on the right-hand side from which the inertial component has been subtracted. It is to be remarked that this condition is satisfied when the estimated added mass $\hat{M}_a$ is greater than at least half the value of the actual viscous added mass M_{av}.

Equation (16) now is to be used in the predictor and corrector steps, which become:

Predictor step

$$\epsilon^{n+\frac{1}{2}} = \epsilon^n + (\Delta t/2)\dot{\epsilon}^n$$

$$\dot{\epsilon}^{n+\frac{1}{2}} = \dot{\epsilon}^n + (\Delta t/2)\ddot{\epsilon}^n \tag{18}$$

$$\ddot{\epsilon}^{n+\frac{1}{2}} = [1/(1+\sigma\hat{M}_a)]\left[-2\zeta\omega_n\dot{\epsilon}^{n+\frac{1}{2}} - \omega_n^2\epsilon^{n+\frac{1}{2}} + \sigma\hat{F}^{n+\frac{1}{2}}\right]$$

Corrector step

$$\epsilon^{n+1} = \epsilon^n + \Delta t\ \dot{\epsilon}^{n+\frac{1}{2}}$$

$$\dot{\epsilon}^{n+1} = \dot{\epsilon}^n + \Delta t\ \ddot{\epsilon}^{n+\frac{1}{2}} \tag{19}$$

$$\ddot{\epsilon}^{n+1} = [1/(1+\sigma\hat{M}_a)]\left[-2\zeta\omega_n\ \dot{\epsilon}^{n+1} - \omega_n^2\epsilon^{n+1} + \sigma\hat{F}^{n+1}\right]$$

in which

$$\hat{F}^{n+1/2} = F\left(\epsilon^{n+\frac{1}{2}},\ \dot{\epsilon}^{n+\frac{1}{2}}\right) + \hat{M}_a\ddot{\epsilon}^{n+\frac{1}{2}} \tag{20}$$

$$\hat{F}^{n+1} = F(\epsilon^{n+1},\ \dot{\epsilon}^{n+1}) + \hat{M}_a\ \ddot{\epsilon}^{n+1} \tag{21}$$

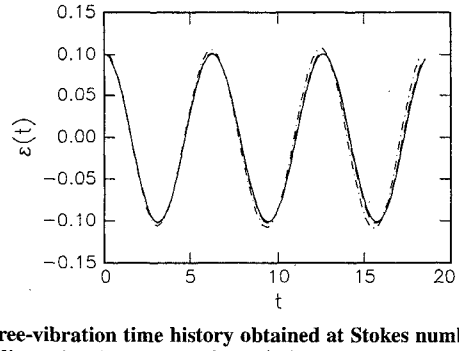

Fig. 4 Free-vibration time history obtained at Stokes number of S = 300 (two-dimensional geometry) for m/m^*_{ap} = 100 and for various time steps: ——, $\Delta t = 2\pi/40$; – – –, $\Delta t = 2\pi/30$; – · –, $\Delta t = 2\pi/20$.

Here $F(\epsilon^{n+\frac{1}{2}}, \dot{\epsilon}^{n+\frac{1}{2}})$ and $F(\epsilon^{n+1}, \dot{\epsilon}^{n+1})$ are obtained as before from the Navier–Stokes equations, whereas $\hat{M}_a\ddot{\epsilon}^{n+\frac{1}{2}}$ and $\hat{M}_a\ddot{\epsilon}^{n+1}$ are calculated by considering the following expressions for the acceleration, used respectively in the predictor step and in the corrector step:

$$\ddot{\epsilon}^{n+1/2} = \left(8\dot{\epsilon}^{n+\frac{1}{2}} - 9\dot{\epsilon}^n + \dot{\epsilon}^{n-1}\right)/(3\ \Delta t)$$
$$\ddot{\epsilon}^{n+1} = (3\dot{\epsilon}^{n+1} - 4\dot{\epsilon}^n + \dot{\epsilon}^{n-1})/(2\ \Delta t) \tag{22}$$

which are consistent with expressions (3) chosen for the fluid acceleration in the Navier–Stokes equations.

This scheme has first been tested for the same two-dimensional problem considered in the last section, and the results, which are referred to as FIC (fluid inertia compensated, as opposed to NFIC, or non–fluid inertia compensated, as used in the previous section), are plotted using dashed lines in Figs. 2 and 3. They are, it is remembered, for a number of values of σ, obtained by varying the ratio of structural mass to potential added mass, m/m^*_{ap}, as per Eq. (14). The added mass estimate $\hat{m}_a$ for that problem was most conveniently selected as the potential value from Eq. (13), which we recall is very close to the actual viscous added mass[4]; hence $\hat{m}_a \equiv m_{ap}$. At $S = 3$, it is seen that the NFIC and FIC curves are perfectly superimposed when $m/m^*_{ap} > 1$, except possibly for $m/m^*_{ap} = 3$ immediately after starting the integration. However, when $m/m^*_{ap} = 1$, in which case, as mentioned previously, the actual viscous added mass is larger than the structural mass m, the FIC results no longer diverge; rather, they are more highly damped than for larger m/m^*_{ap}, as expected. Now, at $S = 300$ in Fig. 3, we again have perfectly superimposed results for $m/m^*_{ap} = 100$, although differences between FIC and NFIC results appear as m/m^*_{ap} decreases, down to the point at $m/m^*_{ap} = 1$, where the two predicted responses are completely different, with divergence predicted by the NFIC calculations, as compared to the physically correct damped oscillations obtained by FIC.

The FIC procedure is seen to require an appropriate estimate for the viscous added mass in any problem with which one is concerned. Since viscous effects have in general very little effect on the determination of the added mass, as has been demonstrated for example in Ref. 4 for the problem under discussion, the viscous added mass may most conveniently be estimated from potential flow calculations. This has been achieved here through Eq. (13), which is the analytical value for the potential added mass, and in more general and complicated problems it may be accomplished, for example, by using finite element potential calculations in which Laplace's equation is solved[9]; this is what has been done in the next section for the three-dimensional annular flow problem. It remains of interest, however, to asses the extent to which different estimates for the viscous added mass would result in the FIC procedure giving different predictions for the dynamic behavior of the system. This question will now be addressed for the two-dimensional annular flow problem by performing calculations with the FIC procedure in which the value of the added mass estimate $\hat{m}_a$ is varied, all other parameters being kept constant.

Thus, calculations have been performed at a Stokes number of $S = 300$, with a constant value of σ obtained from Eq. (14) by setting $m/m^*_{ap} = 1$. The added mass estimate $\hat{m}_a$ was varied by expressing it as a function of the potential added mass m_{ap}, and the results are presented in Fig. 5 for $\hat{m}_a = 0.6m_{ap}$, $\hat{m}_a = m_{ap}$, $\hat{m}_a = 2m_{ap}$, and $\hat{m}_a = 5m_{ap}$, where m_{ap} in all cases is given by Eq. (13). It is seen that, for values of $\hat{m}_a$ not significantly different from the potential value, which itself is to within 10% of the actual viscous added mass at $S = 300$,[4] the FIC method gives results that are only very slightly dependent upon $\hat{m}_a$. Other calculations, not presented here, have established that this is even more so as the ratio of structural mass to fluid-added mass increases, in which case all the curves in Fig. 5 become superimposed and are independent of $\hat{m}_a$; furthermore, the results do not deteriorate as compared to Fig. 5 for very small ratios of structural mass to fluid-added mass.

Thus, the method displays good performance in regard to the selection of the additional parameter that it introduces: Where

structural mass is larger than fluid-added mass the results are largely independent of the added mass estimate; in the contrary case it is sufficient, as mentioned previously, that the estimate be larger than at least half the value of the actual viscous added mass to ensure accuracy of the results (see Fig. 5 for $\hat{m}_a = 0.6m_{ap}$, which just satisfies this condition). The latter condition will be enforced if the added mass estimate is obtained from potential flow calculations.

Application to Three-Dimensional Annular Geometry

We now consider the free vibrations of the cylinder in the three-dimensional geometry of Fig. 1, as obtained after releasing the cylinder from an imposed small initial displacement of $0.1H$; in this case, there is a mean axial flow velocity U in the annular region.

It has been determined in Ref. 4 that the added stiffness is negative for that geometry. We may express the total rigidity of the cylinder plus fluid as being equal to $K + K^*_{av}$, where K and K^*_{av} are, respectively, the dimensional structural and (negative) viscous fluid-added rigidities. Divergence will occur when $K + K^*_{av} < 0$ or, in nondimensional form, when

$$\omega_n^2 + \sigma K_{av} < 0 \tag{23}$$

where ω_n and σ are given by Eq. (8) and $K_{av} = K^*_{av}/\rho U^2 H$. It was found[4] that K_{av} varies little with the Reynolds number for this geometry, with $K_{av} = -483$ at $Re = 50$. Furthermore, the nondimensional potential added mass of the cylinder–fluid system was determined to be equal to $M_{ap} = 91, 100$.[4,9]

Comparisons between FIC and NFIC results are presented in Fig. 6 for $Re = 50$. The mesh on which those calculations were performed had 60 points in the axial direction and 12 points in the radial direction, with the circumferential variable having been eliminated as before using a spectral Galerkin method with Fourier expansions.[4] The dynamics of the cylinder as affected by changes in the value of σ is studied in Fig. 6. Referring to Eq. (8), where ρ and H are constant, varying σ is simply equivalent to changing the structural mass M, this being done in such a way as to also keep ω_n constant and equal to 0.12 in our case; thus structural stiffness K varied proportionately to M [see Eq. (8)]. The corresponding values of σ were calculated from the relation

$$\sigma = \frac{1}{M_{ap}} \frac{1}{M/M^*_{ap}} \tag{24}$$

also valid in three dimensions, and in which M^*_{ap} is the dimensional potential added mass. It is seen in Fig. 6a that for $M/M^*_{ap} = 2$ the system is stable and the corresponding vibrations are damped, as it may be verified that $\omega_n^2 + \sigma K_{av} = 0.012 > 0$; the FIC and NFIC curves are almost perfectly superimposed.

Next, structural mass is diminished such that $M/M^*_{ap} = \frac{2}{3}$. In this case, the system diverges according to the NFIC results in Fig. 6b, even though one still actually has $\omega_n^2 + \sigma K_{av} = 0.006 > 0$; the FIC curve, however, is consistent with the total rigidity of the fluid–cylinder system still being positive and is characteristic of a critically damped, stable system. It is only after a further reduction in M, namely after selecting $M/M^*_{ap} = \frac{2}{9}$, that the FIC calculated system response diverges, as expected, because one then has $\omega_n^2 + \sigma K_{av} = -0.009 < 0$; this is a physical, fluid-elastic divergence, rather than a numerical one.

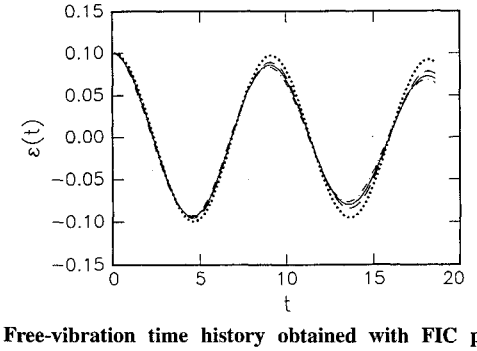

Fig. 5 Free-vibration time history obtained with FIC procedure at Stokes number of $S = 300$ (two-dimensional geometry) for $m/m^*_{ap} = 1$; comparison is made of choice of various added mass estimates: –·–, $\hat{m}_a = 0.6\,m_{ap}$; ——, $\hat{m}_a = m_{ap}$; – – –, $\hat{m}_a = 2\,m_{ap}$; · · ·, $\hat{m}_a = 5\,m_{ap}$.

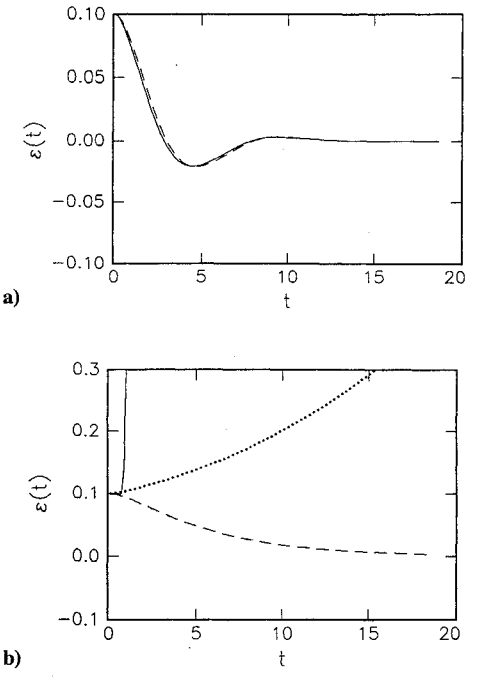

Fig. 6 Free-vibration time history obtained at $Re = 50$ (three-dimensional geometry) for $\omega_n = 0.12$: a) ——, NFIC results; – – –, FIC results for $M/M^*_{ap} = 2$; b) ——, NFIC results; – – –, FIC results for $M/M^*_{ap} = 2/3$; · · ·, FIC results for $M/M^*_{ap} = 2/9$.

Conclusions

It was shown in this paper that a method developed by the authors for the time-marching dynamics analysis of a fluid-coupled structure is numerically unstable when the fluid-added mass is larger than the structural mass. A procedure was devised to fix that anomaly. It consists of introducing an estimate for the fluid-added mass into the structural equation, so as to cancel the fluid inertial forces by transforming them into equivalent structural forces. It was shown that the results are largely independent of the actual value of the added mass estimate, which can be conveniently selected by potential flow calculations. Results obtained from analysis of a cylinder oscillating in annular flow have demonstrated the ability of the proposed method to circumvent the difficulties encountered in the presence of a large added mass.

Acknowledgments

The authors gratefully acknowledge support given to this work by the Natural Sciences and Engineering Research Council of Canada and the Fonds FCAR of Québec and the Commissariat à l'Energie Atomique, France.

References

[1]Nomura, T., and Hughes, T. J. R., "An Arbitrary Lagrangian–Eulerian Finite Element Method for Interaction of Fluid and a Rigid Body," *Computer Methods in Applied Mechanics and Engineering*, Vol. 95, 1992, pp. 115–138.

[2]Rausch, R. D., Batina, J. T., and Yang, H. T. Y., "Three-Dimensional Time-Marching Aeroelastic Analyses Using an Unstructured-Grid Euler Method," *AIAA Journal*, Vol. 31, No. 9, 1993, pp. 1626–1633.

[3]Farhat, C., "Stability Analysis of Dynamic Meshes for Transient Aeroelastic Computations," AIAA Paper 93-3325, 1993.

[4]Bélanger, F., de Langre, E., Axisa, F., Païdoussis, M. P., and Mateescu, D., "Dynamics of Coaxial Cylinders in Laminar Annular Flow by Simultaneous

Integration of the Navier–Stokes and Structural Equations," *Journal of Fluids and Structures*, Vol. 8, 1994, pp. 747–770.

[5]Mateescu, D., Païdoussis, M. P., and Bélanger, F., "Computational Solutions Based on a Finite Difference Formulation for Unsteady Internal Flows," AIAA Paper 91-0724, Jan. 1991.

[6]Rogers, S. E., and Kwak, D., "Upwind Differencing Scheme for the Time-Accurate Incompressible Navier–Stokes Equations," *AIAA Journal*, Vol. 28, 1990, pp. 253–262.

[7]Mateescu, D., Païdoussis, M. P., and Bélanger, F., "Unsteady Annular Viscous Flows Between Oscillating Cylinders. Part 1: Computational Solutions Based on a Time-Integration Method," *Journal of Fluids and Structures*, Vol. 8, 1994, pp. 489–507.

[8]Gibert, R.-J., *Vibrations des Structures*, Editions Eyrolles, Paris, 1988.

[9]De Langre, E., Bélanger, F., and Porcher, G., "Linearized Potential Flow Theory Applied to the Calculation of Fluidelastic Forces in Annular Flow Configurations," *ASME/JSME/IMechE/IAHR 3rd International Symposium on Flow-Induced Vibration and Noise* edited by M. P. Païdoussis et al., Vol. 5, American Society of Mechanical Engineers, New York, 1992.